Graphene Oxide-Based Biosensor for Food Toxin Detection

Saurabh Srivastava · Md Azahar Ali · Sima Umrao ·
Upendra Kumar Parashar · Anchal Srivastava · Gajjala Sumana ·
B. D. Malhotra · Shyam Sudhir Pandey · Shuji Hayase

Abstract We report results of the studies relating to the fabrication of a highly sensitive label free biosensor based on graphene oxide (GO) platform for the detection of aflatoxin B1 (AFB$_1$) which is most toxic and predominant food toxin, using electrochemical impedance spectroscopy. The structural and optical characterization of GO/Au and anti-AFB$_1$/GO/Au has been done by electron microscopy, Raman, X-ray diffraction (XRD), UV–vis and electrochemical impedance spectroscopy (EIS). The impedimetric sensing response of immunoelectrode as a function of AFB$_1$ concentration reveals wider linear detection range (0.5–5 ng/ml), high sensitivity (639 Ω ng^{-1} ml), improved detection limit (0.23 ng ml^{-1}) and good stability (5 weeks) for the label-free detection. Association constant (k_a) for antigen–antibody interaction obtained as 0.46 ng ml^{-1} indicates high affinity.

S. Srivastava · M. A. Ali · G. Sumana · B. D. Malhotra
Department of Science and Technology, Center on Biomolecular Electronics, Biomedical Instrumentation Section, CSIR-National Physical Laboratory, New Delhi 110012, India

S. Srivastava · S. Umrao · A. Srivastava
Department of Physics, Banaras Hindu University, Varanasi, Uttar Pradesh 221005, India

U. K. Parashar
Department of Physics, Indian Institute of Technology Kanpur, Kanpur, Uttar Pradesh 208016, India

B. D. Malhotra (✉)
Department of Biotechnology, Delhi Technological University, Delhi 110042, India
e-mail: bansi.malhotra@gmail.com

S. S. Pandey · S. Hayase
Department of Biological Functions and Systems, Graduate School of Life Science and Systems Engineering, Kyushu Institute of Technology, 2-4, Hibikino, Wakamatsu, Kitakyushu, Japan

Introduction

Graphene, the one-atomic 2D sheet of sp^2-bonded carbon atoms arranged into honeycomb lattice, is emerged as a rapidly rising star in the field of material science. Since its discovery in 2004, graphene-based material has been making a profound impact in many areas of science and technology due to its remarkable physicochemical properties such as high specific surface area (theoretically, 2,630 m^2/g for single-layer graphene), extraordinary electronic properties, strong mechanical strength and excellent thermal and electrical conductivities [13, 2, 30, 1]. One specific branch of graphene research deals with graphene oxide (GO). This can be considered as a precursor for graphene synthesis by either chemical or thermal reduction processes [25, 5]. GO consists of a single layer of graphite oxide and is usually produced by the chemical treatment of graphite through oxidation, with subsequent dispersion and exfoliation in water or suitable organic solvents. Chemically synthesized GO due to its easy and large-scale production, abundant electroactive defects and functional groups, facile surface modification, high surface area, fast electron transfer rate and biocompatibility, has a great potential in the area of electrochemical sensing and biosensing application [36, 11, 7]. The presence of oxygenated functional groups in GO render it strongly hydrophilic and make it highly dispersible in many solvents, including water that allow ease of processing and its modification [32]. The resulting GO-stable dispersion can be subsequently deposited on various conductive substrates in order to make excellent electrodes by means of common methods such as drop-casting, spraying, or spin-coating. In addition, using well-known chemical strategies, these functional groups serve as sites for chemical modification or functionalization of GO, which in turn can be employed to immobilize various electroactive species through covalent or noncovalent bonds for the design of sensitive electrochemical systems. The study of GO-based materials in recent years has been gaining increasing interest due to its facile synthesis, high dispersibility in a range of solvents, capability of coupling electroactive species onto the surface, and unique optical properties for cellular imaging and drug delivery [6, 27].

Electrochemical impedance spectroscopy (EIS) is the study of the resistive and capacitive behavior of the electrode–electrolyte interface in response to a small AC signal whose frequency may be varied over a wide range [14]. EIS is a sensitive, non-destructive and a useful analytical technique extremely sensitive to the biorecognition events happening at the electrode/electrolyte interface [18]. Importantly, EIS has an advantage of label free detection. Usually, labeling of antibody with dye molecules or enzyme (HRP) is used for fluorescence and amperometric sensing, respectively, to achieve high sensitivity. Such labeling processes would not only make experiments relatively complex and expensive, but also affect the binding affinity between the targets and biomolecules to a certain degree. In this regards, EIS provides label free detection with high sensitivity [18, 3, 34, 29].

Aflatoxins (AF) are a group of secondary fungal metabolites that are produced by *Aspergillus flavus* and *Aspergillus parasiticus* under certain conditions and are the most widely spread group of toxins resulting in contamination of food products [4]. There are four main aflatoxins: B_1, B_2, G_1, and G_2. Among these, AFB_1 is known to be most toxic and is responsible for human hepatocellular carcinoma (International Agency for Research on Cancer regards it as a human carcinogen) [9, 4]. Hence, there is an urgent need for availability of a rapid and sensitive detection of AFB_1. Tang et al. utilized multifunctional magnetic bead-based electrochemical immunoassay ($CoFe_2O_4$ nanoparticle as the core and Prussian blue nanoparticle (PBNP)-doped silica as the shell) for the detection of AFB_1 in food. A linear range of 0.05–12 ng/ml was achieved with a detection limit of 6.0 pg/ml [28]. Wang et al. reported a quartz crystal microbalance (QCM)-based biosensor to detect AFB_1 with the detection range of

0.3–7.0 ng/ml, using anti-AFB$_1$-functionalized magnetic core–shell Fe$_3$O$_4$/SiO$_2$ composite nanoparticles, where the bio-functionalized nanoparticles were attached to the surface of the QCM probe with an external magnet [31]. Singh et al. have recently reported a carboxylic multiwalled carbon nanotubes-based electrochemical biosensor for the sensitive detection of AFB$_1$. The biosensor shows high sensitivity of 95 μA/(ng/ml)/cm^2, a detection limit of 0.08 ng/ml in the linear detection range of 0.25–1.375 ng/ml. Additionally, the biosensor shows a good storage stability (42 days) [20]. This report aims towards the efficient and label free detection of AFB$_1$ using the GO-based biosensing platform (Table 1).

Materials and Methods

Materials

Graphite powder flakes (45 μm, >99.99 wt.%), monoclonal anti-AFB$_1$ antibody, AFB$_1$, N-ethyl-N-(3-dimethylaminopropyl)carbodiimide (EDC), N-hydroxysuccinimide (NHS) and bovine serum albumin (BSA) have been procured from Sigma-Aldrich.

Synthesis of Graphene Oxide

GO has been synthesized using modified Hummers method [12] with slight modification. In brief, 1.5 g of graphite powder is pre-oxidized by reacting it with the mixture of 40 ml of 98 % H$_2$SO$_4$, 5 g K$_2$S$_2$O$_8$ and 5 g of P$_2$O$_5$ for 4 h at 80 °C. The resulting suspension is washed with deionized water (DW) four to five times and is vacuum-dried at 50 °C. For the further oxidation pre-oxidized graphite is added to mixture of concentrated H$_2$SO$_4$/H$_3$PO$_4$ (180:13) with constant stirring. After 5 min, 9 g of KMnO$_4$ is added to the mixture and the stirring is continued for 15 h at 50 °C. The reaction is stopped after about 15 h and the reactants are

Table 1 Sensing characteristics of the proposed BSA-anti-AFB$_1$/GO/Au based biosensor compared to some of those reported in literature

Matrix	Sensitivity	Detection limit (ng/ml)	Detection range (ng/ml)	Stability (days)	Ref.
Ni-ITO	59 μA/(ng/ml)	0.327	0.05–1	60	[9]
SPCE	–	0.15	0.05–2	30	[17]
Au NPs	1.4 μS/(ng/ml)	0.1	0.5–10	12	[10]
Au Nps/PTH-GCE	1.23 μA/(ng/ml)	0.07	0.6–2.4		[15]
MMB	46 nA/(ng/ml)	0.006	0.05–12	17	[28]
Au/TiO$_2$/RTIL/Nafion/GCE	0.12 μA/(ng/ml)	0.05	0.1–12	19	[26]
RGO/ITO	68 μA/(ng/ml)	0.15	0.125–1.5	45	[23]
MWCNTs/ITO	95 μA/(ng/ml)	0.08	0.25–1.37	42	[20]
Pt/PANi–PSSA	869.6Ω ng^{-1} ml	100	1–6	–	[16]
Nanogold colloid (fluorescence based)	–	2.5	–	–	[33]
CdTe QDs (fluorescence based)	–	6.25×10^{-3}	31.2–187.4×10^3	–	[35]
GO/Au	639Ω ng^{-1} ml	0.23	0.5–5	35	Present work

allowed to cool at room temperature after which 200 ml of ice has been poured into mixture followed by 1.5 ml of H_2O_2 (30 %). The fine material from the mixture is separated through U.S. standard testing sieve of pore size 30 μm and finally the filtration is done. The supernatant is discarded and the filtrate is subjected to centrifugation at 5,000 rpm for about 30 min. After that multiple washing of the sediment material has been carried out using distilled water, dilute HCl and ethanol (100 ml of each) followed by centrifugation separation. The final sediment is suspended in 100 ml of ether and is filtered through PTFE membrane with a pore size of 0.45 μm. The semisolid material obtained as GO is vacuum-dried overnight. The solid brown powder as GO is thus obtained.

Preparation of GO/Au Film

Gold electrodes (1.5×0.5 cm^2) are cleaned with piranha solution ($7H_2SO_4/3H_2O_2$). Ten microlitres of the aqueous GO solution (1 mg/ml) is uniformly spread onto Au electrodes followed by drying at 50 °C in vacuum oven overnight. The resulting GO/Au electrodes have been utilized for the immobilization of antibodies molecules.

Biofunctionalization of GO/Au Electrode Surface with Anti-AFB$_1$

Prior to the covalent immobilization process, COOH group of GO/Au electrode has been activated using EDC as the coupling agent and NHS as an activator [24]. The anti-AFB$_1$ antibody solution (10 μg/ml) is freshly prepared in phosphate buffer saline (PBS; pH 7.4). Then, 10 μl of this solution is uniformly spread on the activated GO/Au electrode surface and is incubated in humid chamber for about 4 h. The covalent interaction occurs via the formation of strong amide (CO–NH) bond between carboxyl group of GO and amino terminal of the anti-AFB$_1$. The anti-AFB$_1$/GO/ITO immunoelectrode is washed with PBS to remove the unbound antibodies molecules. Further the immunoelectrode is treated with BSA solution (1 mg/ml) which acts as a blocking agent for the non-specific active sites present on the electrode surface. The BSA-anti-AFB$_1$/GO/ITO immunoelectrode is then washed with PBS and stored at 4 °C, when not in use.

Results and Discussion

Structural Studies

Figure 1a shows powder X-ray diffraction (XRD) pattern (copper Kα radiation) of GO and in the range of 5–80°. The intense peak seen at 11.3° (7.96 Å) corresponds to the plane (002) and another peak found at 42.1° (2.12 Å) for the reflection plane (001) of GO (curve a). The number of layers (seven) of the GO has been obtained using the Debye–Scherrer equation [19, 22]

$$t = 0.89\lambda/\beta_{002}\cdot\cos\theta_{002} \qquad (1)$$

$$n = t/d_{002}, \qquad (2)$$

where t is thickness, β_{002} is the full width at half-maximum (FWHM), n is the number of graphene layers and d_{002} is interlayer spacing.
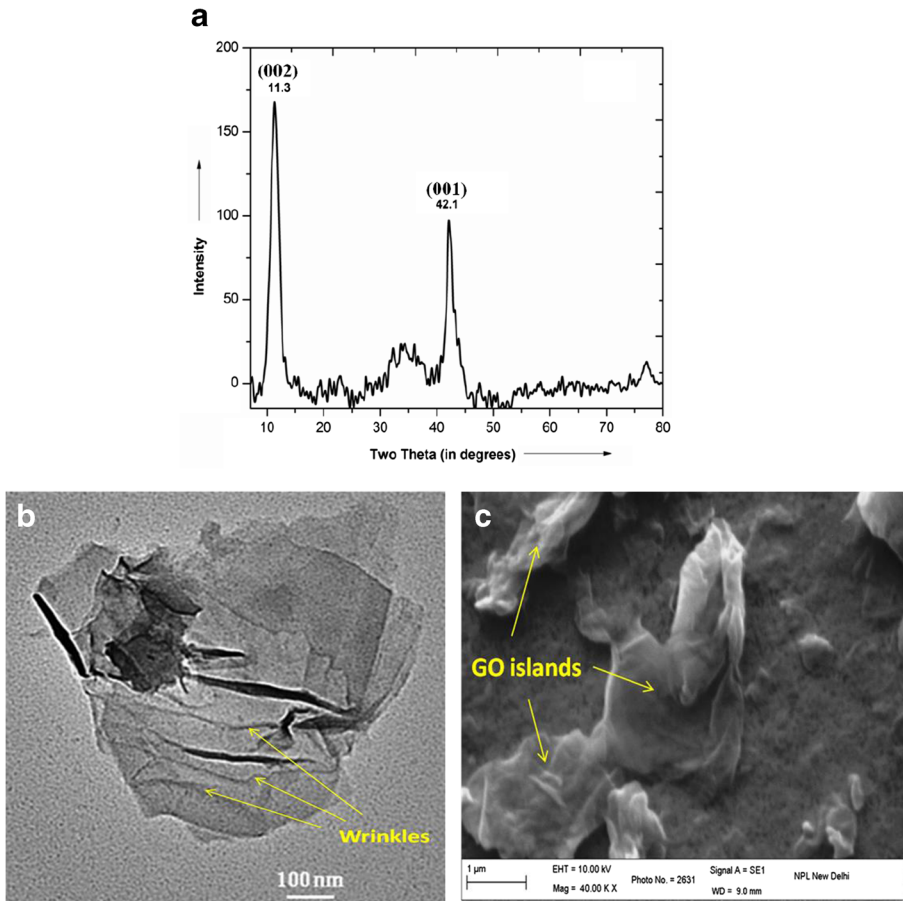
Fig. 1 a XRD pattern of graphene oxide shows the characteristic peaks at 11.3° corresponding to (002) plane. **b** Transmission electron micrograph of the graphene oxide indicating wrinkles and folding on the graphene sheets. **c** Scanning electron micrograph of graphene oxide film deposited onto Au electrode by drop cast method

Figure 1b shows the transmission electron micrograph (TEM) of GO. For TEM studies, well suspended GO has been prepared in water and drop casted onto carbon-coated copper grid. The image clearly demonstrates overlapped graphene layers and the folds and wrinkles are clearly visible. Some of the portion appears darker indicating more graphene sheets than the brighter region.

Figure 1c shows the scanning electron micrograph (SEM) of the GO/Au electrode surface, wherein micron sized island of GO sheet instead of a homogeneous layer clearly appears. It implies that the individual graphene sheets stack together to form larger sheets in the form of flake-like structures.

Optical Studies

Figure 2a indicates UV–vis spectroscopic studies of GO that has been carried out in wavelength range of 200–900 nm. The absorption of radiation starts increasing at 350 nm, wherein the maximum absorption has been seen at 226 nm. This may be assigned due to π–π*
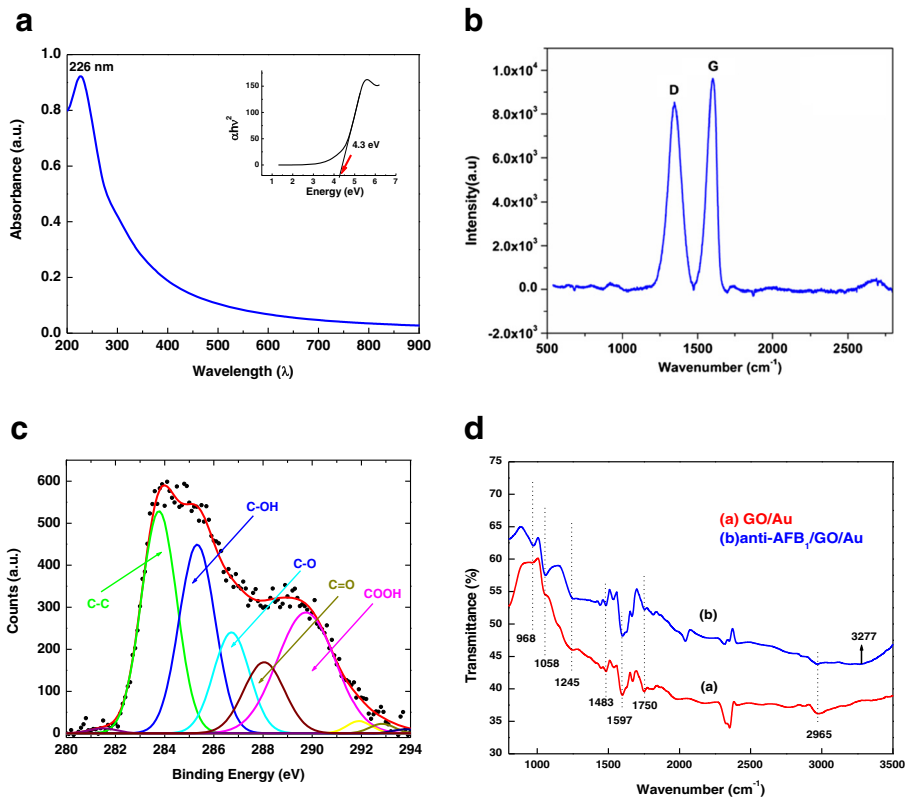
Fig. 2 **a** UV–visible spectra of graphene oxide indicating the maximum absorption seen at 226 nm corresponding to π–π* transition of aromatic C–C bonds. *Inset*: plot of $(\alpha h\nu)^2$ versus $h\nu$ for the estimation of optical band gap (4.11 eV). **b** Raman spectrum of graphene oxide. **c** X-ray photoelectron spectrum (*XPS*) of the C1s region of graphene oxide. **d** FTIR of GO/Au and anti-AFB$_1$/GO/Au film. The additional amide band seen at 3,277 cm^{-1} and reduction in the intensity of band seen at 2,977 cm^{-1} confirms the covalent immobilization of the antibody molecules

transition of aromatic C–C bonds in GO. The band gap of GO is found to be 4.3 eV estimated using the Tauc equation [21].

Figure 2b demonstrates Raman spectra of GO wherein well-defined D, G and 2D bands are observed. The prominent *D* peak may be seen at 1,348 cm^{-1}, which indicates the presence of disorder in the GO structure. This can be assigned to both the structural disorder (induced by the tears and folding over of the graphene sheets) and the presence of residual oxygen as well as point defects [8]. The G band seen at 1,598 cm^{-1} represents the planar sp^2 bonded carbon of GO. 2D band (overtone of the D band) found at 2,678 cm^{-1} is due to the second harmonic of D band indicating dispersive character as a function of excitation energy.

Figure 2c shows XPS spectrum of C 1 s region of the synthesized GO. The spectrum has been deconvoluted into the characteristic binding energy peaks using peak fit 1 software. Background subtraction and peak fitting of the spectra have been done using the Shirley function and Gaussian function, respectively. XPS measurements have been carried out in a Perkin Elmer XPS chamber (PHI 1257) with a base pressure of 5×10^{-9} Torr. The chamber is equipped with a dual anode Mg-K$_\alpha$(energy 1,253.6 eV) and Al-K$_\alpha$(energy 1,486.6 eV) X-ray source and a high-resolution hemispherical energy analyzer for energy resolved electron detection. An Mg-K$_\alpha$X-ray source has been used for this study. The samples are sputtered

with 4 keV argon ions to remove surface contamination prior to XPS studies. The binding energy peak found at 283.7 eV is assigned to graphitic C–C bond. The binding energy peaks seen at 285.3 and 286.7 eV is due to the hydroxyl (C–OH) and epoxy (C–O) groups, respectively. Furthermore, the binding energy peak seen at 288 and 289.7 eV can be attributed to the carbonyl (C=O) and carboxylic acid (O–C=O) groups present in the samples [23]. Table 2 indicates the binding energy position of the various functional groups, FWHM and the corresponding relative percentage of these groups in the GO. These results indicate that the GO has abundant carboxylic acid functional groups as evident by their high relative atomic percentage (24.1 %). These carboxylic acid groups have been used to bind with amino terminal of the antibodies through the covalent immobilization process.

Figure 2d shows Fourier transform infrared spectra (FTIR) of the (a) GO/Au and (b) anti-AFB$_1$/GO/Au. The bands observed at 968 cm^{-1} represents the C–H stretching vibrations. The bands seen at 1,058 cm^{-1} represent the C–O–C stretching vibration of the epoxy group present in the GO. The band seen at 1,245 cm^{-1} represents the C–OH stretching vibrations of the hydroxyl group. The characteristic band observed at 1,750 cm^{-1} may be assigned to C=O stretching vibrations of the carboxylic/carbonyl groups present in the GO. The characteristic band seen at 1,597 cm^{-1} is due to the aromatic C=C stretching vibration, while a band seen at 1,483 cm^{-1} represents the H–C–H bending vibrations. Further, band at 2,965 cm^{-1} is due to the O–H stretch of the carboxylic acid group, the intensity of which get reduced after antibody immobilization (curve b). It indicates that the COOH group gets utilized in the formation of amide bond with antibodies molecules. Moreover, the additional band seen at around 3,277 cm^{-1} represents N–H stretching of the amide A (curve b).

Electrochemical Impedance Spectroscopic Studies

Figure 3a shows the Nyquist plot obtained for bare Au, GO/Au, anti-AFB$_1$/GO/Au and BSA/anti-AFB$_1$/GO/Au electrodes in the PBS containing 5 mM [Fe(CN)$_6$]$^{4-/3}$ in the frequency range 10^6–10^{-1} Hz at biasing potential of 10 mV. The charge transfer process in these electrodes has been investigated by measuring charge transfer resistance (R_{ct}) at the electrode/electrolyte interface. The value of the charge transfer resistance (R_{ct}) depends on the dielectric and insulating features at the electrode/electrolyte interface. It has been observed that magnitude of R_{ct} for Au electrode (312 Ω, curve a) increases to 363 Ω after its modification with GO. It may be attributed to the insulating characteristic of GO that reduces the conductivity of the gold surface (curve b). The R_{ct} value obtained for anti-AFB$_1$/GO/Au been found to enhance significantly up to 968 Ω. It is because the antibody molecules form an insulating layer on the electrode surface and creates hindrance in the electron transfer to the electrode surface. Further, the R_{ct} value, in the case of BSA-treated immunoelectrode (BSA/anti-AFB$_1$/GO/Au), increases to 1,122 Ω. It is because of the fact that BSA acts as blocking agent which blocks most of the non-specific active sites of the immunoelectrode surface.

Table 2 The C 1 s peak position, FWHM and the relative atomic percentage of various functional groups of the synthesized graphene oxide

| Functional groups	Binding energy (eV)	FWHM (eV)	Relative percentage (%)
C–C	283.7	1.69	27.16
C–OH	285.3	1.72	23.45
C–O	286.7	1.72	12.54
C=O	288	1.58	9.99
O–C=O	289.7	2.6	24.13

Response Studies

EIS response studies of the BSA-anti-AFB$_1$/GO/Au immunoelectrode have been investigated as a function of AFB$_1$ concentration (0.5–5 ng/ml) using the EIS technique. Figure 3b indicates the Nyquist plot obtained for the immunoelectrode as a function of AFB$_1$ concentration. It has been observed that the charge transfer resistance (R_{ct}) increases with respect to the AFB$_1$ concentration. This is because the formation of antigen–antibody complexes reduces the conductivity of electrode surface and acts as a barrier in the electron transfer process. Figure 3b shows the calibration plot of R$_{ct}$ values obtained for BSA-anti-AFB$_1$/GO/Au immunoelectrode as a function of the AFB$_1$ concentration. The linear variation of the R$_{ct}$ value with AFB$_1$ concentrations (0.5–5 ng ml^{-1}) obeys Eq. 3.

$$R_{ct}(\Omega) = 783\,(\Omega) + 319.5\,(\Omega ng^{-1} ml) * \left[concentration\,(ng\,ml^{-1}) \right] \qquad (3)$$

Regression coefficient (R^2)=0.99.

This GO/Au-based immunosensor shows high sensitivity of $639\,\Omega$ ng^{-1} ml cm^{-2} and linear detection range as 0.5–5 ng ml^{-1}. The limit of detection has been evaluated using $3\sigma/m$ criteria,
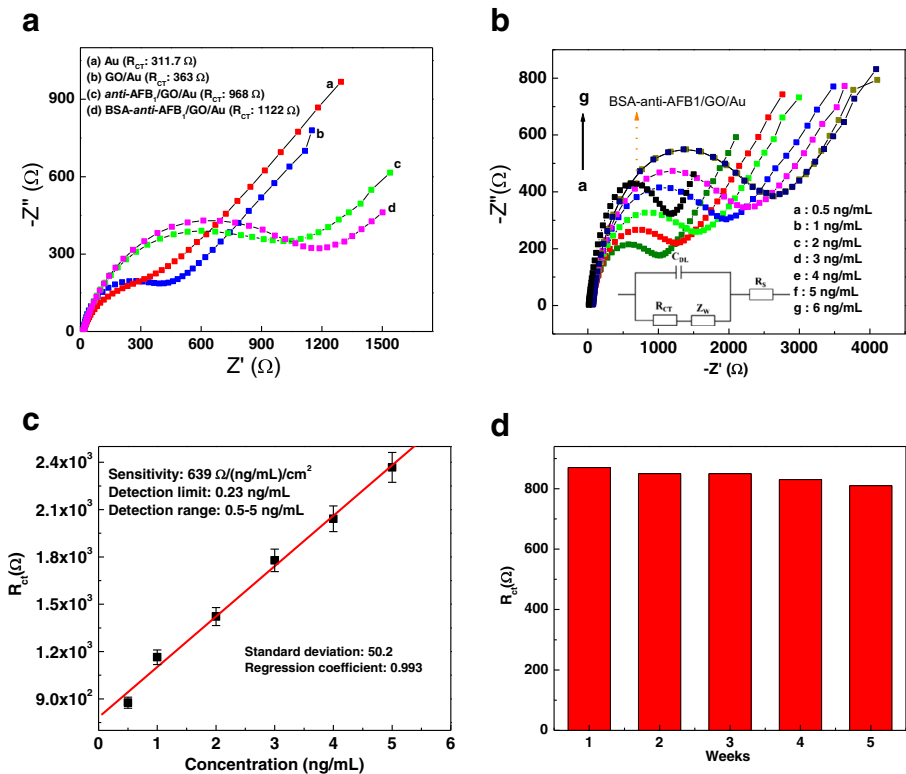
Fig. 3 **a** EIS (Nyquist plot) of various modified electrodes, obtained in PBS (pH 7.4) containing 5 mM [Fe(CN)$_6$]$^{3-/4-}$. **b** EIS response of the BSA-anti-AFB$_1$/GO/Au immunoelectrode obtained as a function of AFB$_1$ concentration. **c** Calibration plot between the magnitude of the charge transfer resistance (R_{ct}) and AFB$_1$ concentrations (0.5–5 ng ml^{-1}). **d** Plot of R_{ct} as a function of time indicating good storage stability of the biosensor (5 weeks)

where σ is the standard deviation and m is the sensitivity of calibration plot, and is found to be 0.23 ng ml^{-1}. The value of the association constant (K_a) obtained as 0.46 ng ml^{-1} using a Hanes–Woolf plot that indicates high affinity of AFB$_1$ towards anti-AFB$_1$. Furthermore, the large available surface area and abundant functional groups (carboxylic) of the graphene sheets provides high loading of anti-AFB$_1$ molecules resulting in wider linear detection range as well as high sensitivity. The storage stability of this BSA-anti-AFB$_1$/GO/Au-based impedimetric biosensor has been investigated by observing the charge transfer resistance (R_{ct}) at a regular interval of 1 week for 5 weeks with 1 ng/ml concentration of AFB$_1$ (Fig. 3d). Results of these studies indicate no significant decrease in the R_{ct} value (within 5 %) even after 5 weeks, revealing its good storage stability. The sensing performance of the proposed BSA-anti-AFB$_1$/GO/Au-based biosensor is summarized in Table 1 along with some of those reported in the literature.

We compared the EIS response of GO-based (BSA-anti-AFB$_1$/GO/Au) immunoelectrodes to that of Au (BSA-anti-AFB$_1$/Au) and graphite (BSA-anti-AFB$_1$/graphite/Au) in order to show the advantage of GO to the other two counterparts, for the detection of AFB$_1$ food toxin. Since both Au and graphite electrode surface have no functional groups, covalent immobilization of AFB$_1$ cannot be achieved. The anti-AFB$_1$ antibody molecules are physically adsorbed on Au as well as graphite electrode surface and then treated with BSA solution (1 mg/ml). Figure S1a shows the EIS response of the BSA-anti-AFB$_1$/Au immunoelectrode obtained as a function of AFB$_1$ concentration. Here, we do not observe any significant change in the Rct value for AFB$_1$ concentrations (0.5, 1 and 2 ng/ml). It has also been observed that above 2 ng/ml AFB$_1$ concentration, the EIS response saturates (Nyquist plots coincide). This may be due to the poor binding affinity of AFB$_1$ and Au. Figure S1b shows EIS response of the BSA-anti-AFB$_1$/graphite/Au immunoelectrode obtained as a function of AFB$_1$ concentration. Figure S1c shows calibration plot between the magnitude of the charge transfer resistance (R$_{ct}$) and AFB$_1$ concentrations (0.5–4 ng ml^{-1}). However, the response is found to be linear in the range of (1–4 ng/ml) (inset, Fig. S1c)]. The detection sensitivity estimated from the slope of linear calibration plot, in case of BSA-anti-AFB$_1$/graphite/Au immunoelectrode has been estimated as 74Ω ng^{-1} ml cm^{-2}, which is lower than that of BSA-anti-AFB$_1$/GO/Au (639Ω ng^{-1} ml cm^{-2}). This BSA-anti-AFB$_1$/graphite/Au shows detection limit of 0.7 ng/ml, which is higher than that of BSA-anti-AFB$_1$/GO/Au (0.23 ng/ml). It is also clear that GO-based immuosensor shows a wider linear detection range of 0.5–5 ng/ml as compared to graphite (1–4 ng/ml) and gold (0.5–2 ng/ml) electrodes. So, these studies clearly reveals the advantage of GO to the other two counterparts namely Au and graphite, in terms of sensing characteristics of the biosensor for the detection of food toxin (AFB$_1$).

Conclusions

GO has been synthesized using modified Hummers method and used to form thin film GO/Au electrode. The GO/Au electrode has been utilized for the covalent immobilization of the monoclonal antibody molecules (anti-AFB$_1$) using EDC-NHS protocol. The anti-AFB$_1$/GO/Au immunoelectrode has been successfully used as a label free biosensing platform to detect a range of AFB$_1$ concentration employing EIS. The fabricated impedimetric immunosensor shows wider linear detection range (0.5–5 ng/ml) along with high sensitivity (639Ω/(ng/ml)/cm^2) and good storage stability (5 weeks). In addition, this GO-based biosensing platform may efficiently be utilized for the label free detection of other important food toxins such as aflatoxin M$_1$ and ochratoxin-A.

References

1. Alwarappan, S., Erdem, A., Liu, C., & Li, C.-Z. (2009). Probing the electrochemical properties of graphene nanosheets for biosensing applications. *Journal of Physical Chemistry C, 113*, 8853–8857.
2. Balandin, A. A. (2011). Thermal properties of graphene and nanostructured carbon materials. *Nature Materials, 10*, 569–581.
3. Bart, M., Stigter, E., Stapert, H., De Jong, G., & Van Bennekom, W. (2005). On the response of a label-free interferon-γ immunosensor utilizing electrochemical impedance spectroscopy. *Biosensors and Bioelectronics, 21*, 49–59.
4. Daly, S. J., Keating, G. J., Dillon, P. P., Manning, B. M., O'Kennedy, R., Lee, H. A., & Morgan, M. R. A. (2000). Development of surface plasmon resonance-based immunoassay for aflatoxin B1. *Journal of Agricultural and Food Chemistry, 48*, 5097–5104.
5. Dikin, D. A., Stankovich, S., Zimney, E. J., Piner, R. D., Dommett, G. H., Evmenenko, G., Nguyen, S. T., & Ruoff, R. S. (2007). Preparation and characterization of graphene oxide paper. *Nature, 448*, 457–460.
6. Dong, H., Gao, W., Yan, F., Ji, H., & Ju, H. (2010). Fluorescence resonance energy transfer between quantum dots and graphene oxide for sensing biomolecules. *Analytical Chemistry, 82*, 5511–5517.
7. Dreyer, D. R., Park, S., Bielawski, C. W., & Ruoff, R. S. (2010). The chemistry of graphene oxide. *Chemical Society Reviews, 39*, 228–240.
8. Eda, G., Fanchini, G., & Chhowalla, M. (2008). Large-area ultrathin films of reduced graphene oxide as a transparent and flexible electronic material. *Nature Nanotechnology, 3*, 270–274.
9. Kalita, P., Singh, J., Singh, M. K., Solanki, P. R., Sumana, G., & Malhotra, B. D. (2012). Ring like self assembled Ni nanoparticles based biosensor for food toxin detection. *Applied Physics Letters, 100*, 093702–093704.
10. Liu, Y., Qin, Z., Wu, X., & Jiang, H. (2006). Immune-biosensor for aflatoxin B1 based bio-electrocatalytic reaction on micro-comb electrode. *Biochemical Engineering Journal, 32*, 211–217.
11. Liu, Y., Yu, D., Zeng, C., Miao, Z., & Dai, L. (2010). Biocompatible graphene oxide-based glucose biosensors. *Langmuir, 26*, 6158–6160.
12. Chen, C., Li, J., Li, R., Xiao, G., & Yan, D. (2013). Synthesis of superior dispersions of reduced graphene oxide. *New Journal of Chemistry, 37*, 2778–2783.
13. Neto, A. C., Guinea, F., Peres, N., Novoselov, K. S., & Geim, A. K. (2009). The electronic properties of graphene. *Reviews of Modern Physics, 81*, 109.
14. Orazem, M. E. and Tribollet, B. (2011) *Electrochemical impedance spectroscopy.* Wiley.
15. Owino, J., Arotiba, O., Hendricks, N., Songa, E., Jahed, N., Waryo, T., Ngece, R., Baker, P., & Iwuoha, E. (2008). Electrochemical immunosensor based on polythionine/gold nanoparticles for the determination of aflatoxin B1. *Sensors, 8*, 8262–8274.
16. Owino, J. H., Ignaszak, A., Al-Ahmed, A., Baker, P. G., Alemu, H., Ngila, J. C., & Iwuoha, E. I. (2007). Modelling of the impedimetric responses of an aflatoxin B1 immunosensor prepared on an electrosynthetic polyaniline platform. *Analytical and Bioanalytical Chemistry, 388*, 1069–1074.
17. Piermarini, S., Micheli, L., Ammida, N. H. S., Palleschi, G., & Moscone, D. (2007). Electrochemical immunosensor array using a 96-well screen-printed microplate for aflatoxin B1 detection. *Biosensors and Bioelectronics, 22*, 1434–1440.
18. Ruan, C., Yang, L., & Li, Y. (2002). Immunobiosensor chips for detection of *Escherichia coli* O157: H7 using electrochemical impedance spectroscopy. *Analytical Chemistry, 74*, 4814–4820.
19. Sakintuna, B., Yürüm, Y., & Çetinkaya, S. (2004). Evolution of carbon microstructures during the pyrolysis of Turkish Elbistan lignite in the temperature range 700−1000 °C. *Energy & Fuels, 18*, 883–888.
20. Singh, C., Srivastava, S., Ali, M. A., Gupta, T. K., Sumana, G., Srivastava, A., Mathur, R., & Malhotra, B. D. (2013). Carboxylated multiwalled carbon nanotubes based biosensor for aflatoxin detection. *Sensors and Actuators B: Chemical, 185*, 258–264.
21. Singh, M. K., Mathpal, M. C., & Agarwal, A. (2012). Optical properties of SnO$_2$ quantum dots synthesized by laser ablation in liquid. *Chemical Physics Letters, 536*, 87–91.
22. Srivastava, R. K., Srivastava, S., Narayanan, T. N., Mahlotra, B. D., Vajtai, R., Ajayan, P. M., & Srivastava, A. (2011). Functionalized multilayered graphene platform for urea sensor. *ACS Nano, 6*, 168–175.

23. Srivastava, S., Kumar, V., Ali, M. A., Solanki, P. R., Srivastava, A., Sumana, G., Saxena, P. S., Joshi, A. G., & Malhotra, B. (2013). Electrophoretically deposited reduced graphene oxide platform for food toxin detection. *Nanoscale, 5*, 3043–3051.
24. Srivastava, S., Solanki, P. R., Kaushik, A., Ali, M. A., Srivastava, A., & Malhotra, B. D. (2011). A self assembled monolayer based microfluidic sensor for urea detection. *Nanoscale, 3*, 2971–2977.
25. Stankovich, S., Dikin, D. A., Piner, R. D., Kohlhaas, K. A., Kleinhammes, A., Jia, Y., Wu, Y., Nguyen, S. T., & Ruoff, R. S. (2007). Synthesis of graphene-based nanosheets via chemical reduction of exfoliated graphite oxide. *Carbon, 45*, 1558–1565.
26. Sun, A.-L., Qi, Q.-A., Dong, Z.-L., & Liang, K. (2008). An electrochemical enzyme immunoassay for aflatoxin B$_1$ based on bio-electrocatalytic reaction with room-temperature ionic liquid and nanoparticle-modified electrodes. *Sensing and Instrumentation for Food Quality and Safety, 2*, 43–50.
27. Sun, X., Liu, Z., Welsher, K., Robinson, J. T., Goodwin, A., Zaric, S., & Dai, H. (2008). Nano-graphene oxide for cellular imaging and drug delivery. *Nano Research, 1*, 203–212.
28. Tang, D., Zhong, Z., Niessner, R., & Knopp, D. (2009). Multifunctional magnetic bead-based electrochemical immunoassay for the detection of aflatoxin B1 in food. *Analyst, 134*, 1554–1560.
29. Tang, H., Chen, J., Nie, L., Kuang, Y., & Yao, S. (2007). A label-free electrochemical immunoassay for carcinoembryonic antigen (CEA) based on gold nanoparticles (AuNPs) and nonconductive polymer film. *Biosensors and Bioelectronics, 22*, 1061–1067.
30. Wang, C., Li, D., Too, C. O., & Wallace, G. G. (2009). Electrochemical properties of graphene paper electrodes used in lithium batteries. *Chemistry of Materials, 21*, 2604–2606.
31. Wang, L., & Gan, X.-X. (2009). Biomolecule-functionalized magnetic nanoparticles for flow-through quartz crystal microbalance immunoassay of aflatoxin B1. *Bioprocess and Biosystems Engineering, 32*, 109–116.
32. Wang, Y., Li, Z., Wang, J., Li, J., & Lin, Y. (2011). Graphene and graphene oxide: biofunctionalization and applications in biotechnology. *Trends in Biotechnology, 29*, 205–212.
33. Xiulan, S., Xiaolian, Z., Jian, T., Zhou, J., & Chu, F. (2005). Preparation of gold-labeled antibody probe and its use in immunochromatography assay for detection of aflatoxin B1. *International Journal of Food Microbiology, 99*, 185–194.
34. Yang, L., Li, Y., & Erf, G. F. (2004). Interdigitated array microelectrode-based electrochemical impedance immunosensor for detection of *Escherichia coli* O157: H7. *Analytical Chemistry, 76*, 1107–1113.
35. Zekavati, R., Safi, S., Hashemi, S. J., Rahmani-Cherati, T., Tabatabaei, M., Mohsenifar, A., & Bayat, M. (2013). Highly sensitive FRET-based fluorescence immunoassay for aflatoxin B1 using cadmium telluride quantum dots. *Microchimica Acta, 180*, 1217–1223.
36. Zhou, M., Zhai, Y., & Dong, S. (2009). Electrochemical sensing and biosensing platform based on chemically reduced graphene oxide. *Analytical Chemistry, 81*, 5603–5613.